

# Kepler-6b: A Transiting Hot Jupiter Orbiting a Metal-Rich Star<sup>†</sup>

Edward W. Dunham<sup>1</sup>, William J. Borucki<sup>2</sup>, David G. Koch<sup>2</sup>, Natalie M. Batalha<sup>3</sup>,  
Lars A. Buchhave<sup>4,5</sup>, Timothy M. Brown<sup>6</sup>, Douglas A. Caldwell<sup>7</sup>, William D. Cochran<sup>8</sup>,  
Michael Endl<sup>8</sup>, Debra Fischer<sup>17</sup>, Gabor Fűrész<sup>4</sup>, Thomas N. Gautier III<sup>9</sup>, John C. Geary<sup>4</sup>,  
Ronald L. Gilliland<sup>10</sup>, Alan Gould<sup>16</sup>, Steve B. Howell<sup>11</sup>, Jon M. Jenkins<sup>7</sup>, Hans Kjeldsen<sup>15</sup>,  
David W. Latham<sup>4</sup>, Jack J. Lissauer<sup>2</sup>, Geoffrey W. Marcy<sup>12</sup>, Soren Meibom<sup>4</sup>,  
David G. Monet<sup>13</sup>, Jason F. Rowe<sup>14,7</sup>, Dimitar D. Sasselov<sup>4</sup>

## ABSTRACT

---

<sup>†</sup>Based in part on observations obtained at the W. M. Keck Observatory, which is operated by the University of California and the California Institute of Technology.

<sup>1</sup>Lowell Observatory, Flagstaff, AZ 86001

<sup>2</sup>NASA Ames Research Center, Moffett Field, CA 94035

<sup>3</sup>San Jose State University, San Jose, CA 95192

<sup>4</sup>Harvard-Smithsonian Center for Astrophysics, Cambridge, MA 02138

<sup>5</sup>Niels Bohr Institute, Copenhagen University, DK-2100 Copenhagen, Denmark

<sup>6</sup>Las Cumbres Observatory Global Telescope, Goleta, CA 93117

<sup>7</sup>SETI Institute, Mountain View, CA 94043

<sup>8</sup>University of Texas, Austin, TX 78712

<sup>9</sup>Jet Propulsion Laboratory/California Institute of Technology, Pasadena, CA 91109

<sup>10</sup>Space Telescope Science Institute, Baltimore, MD 21218

<sup>11</sup>National Optical Astronomy Observatory, Tucson, AZ 85719

<sup>12</sup>University of California, Berkeley, Berkeley, CA 94720

<sup>13</sup>US Naval Observatory, Flagstaff Station, Flagstaff, AZ 86001

<sup>14</sup>NASA Postdoctoral Program Fellow

<sup>15</sup>University of Aarhus, Aarhus, Denmark

<sup>16</sup>Lawrence Hall of Science, Berkeley, CA 94720

<sup>17</sup>Yale University, New Haven, CT 06510

We announce the discovery of Kepler-6b, a transiting hot Jupiter orbiting a star with unusually high metallicity,  $[\text{Fe}/\text{H}] = +0.34 \pm 0.04$ . The planet’s mass is about 2/3 that of Jupiter,  $M_{\text{P}} = 0.67 M_{\text{J}}$ , and the radius is thirty percent larger than that of Jupiter,  $R_{\text{P}} = 1.32 R_{\text{J}}$ , resulting in a density of  $\rho_{\text{P}} = 0.35 \text{ g cm}^{-3}$ , a fairly typical value for such a planet. The orbital period is  $P = 3.235$  days. The host star is both more massive than the Sun,  $M_{\star} = 1.21 M_{\odot}$ , and larger than the Sun,  $R_{\star} = 1.39 R_{\odot}$ .

*Subject headings:* planetary systems — stars: individual (Kepler-6, KIC 10874614, 2MASS 19472094+4814238) — techniques: spectroscopic

## 1. INTRODUCTION

The *Kepler* mission was launched on March 6, 2009 to undertake a search for Earth-size planets orbiting in the habitable zones of stars similar to the Sun. *Kepler* uses the transit photometry approach for this task (Borucki et al. 2010a). *Kepler*’s commissioning process went very well and the system is providing data of exceptional photometric quality (Koch et al. 2010a). Indeed, the final commissioning data, 9.7 days of science-like observations of 50000 stars selected from the *Kepler Input Catalog* (KIC) (Koch et al. 2010a), were of such high quality that they are now commonly, if incorrectly, referred to as the “quarter 0” data. A number of *Kepler* Objects of Interest (KOIs) simply fell out of this dataset, including the present object, known as KOI-17. Its transit signal is huge by *Kepler* standards, and excellent light curve results were obtained quickly. The follow-up spectroscopic observations took somewhat longer since observations were not planned to be undertaken so soon after commissioning. As a result the first data intended for science, 33.5 days of observations of 150000 KIC stars, became available in the meantime and were folded in with the original test data for the analysis presented here. The 1.3 day gap between these two sets of data contained one transit of Kepler-6b. Haas et al. (2010) provide additional details regarding the *Kepler* data used in this analysis.

Because the pace of early *Kepler* extrasolar planet discoveries is limited by the radial-velocity follow-up observations, the first objects to be announced tend to be those most easily confirmed spectroscopically. Kepler-6b (= KIC 10874614,  $\alpha = 19^{\text{h}}47^{\text{m}}20^{\text{s}}.94$ ,  $\delta = +48^{\circ}14'23''.8$ , J2000, KIC  $r = 13.253$  mag) is one of these objects.

## 2. KEPLER PHOTOMETRY

The *Kepler* science data for the primary transit search mission are the long cadence data (Jenkins et al. 2010a). These consist of sums very nearly 30 minutes in length (with rigorously the same integration time) of each pixel in the aperture containing the target star in question. These data proceed through an analysis pipeline to produce corrected pixel data, then simple unweighted aperture photometry sums are formed to produce a photometric time series for each object (Jenkins et al. 2010b). The many thousands of photometric time series are then processed by the transiting planet search (TPS) pipeline element (Jenkins et al. 2010b). The candidate transit events identified by TPS were then vetted by visual inspection.

The light curves produced by the photometry pipeline tend to show drifts due to an extremely small, slow focus change (Jenkins et al. 2010a), and there are also sometimes low frequency variations in the stellar signal that can make analysis of the transit somewhat problematic. These low frequency effects can be removed by modest filters that have only an insignificant effect on the transit signal (Koch et al. 2010b). The unfolded and folded light curves for Kepler-6b produced in this manner are shown in Figure 1. <sup>1</sup>

Figure 1 illustrates two of the ways we reject false positives based on the *Kepler* light curves alone. The lower part of the figure shows the planetary transit (referred to the left ordinate). The points marked with + and × symbols refer to alternating even and odd transit events. This aids in detecting eclipsing binary stars with nearly, but not quite equal primary and secondary minima. No such deviation is observed for Kepler-6. The upper curve shows the time of secondary minimum, assuming zero eccentricity. The vertical scale, on the right, is magnified and measured in parts per million to help search for a small secondary minimum that might be due to occultation of an M dwarf companion. Again, no such signature is visible.

## 3. FOLLOW-UP OBSERVATIONS

The crucial importance of ground-based follow-up observations was recognized long ago (Latham 2003) and a well-established plan was in place by the time of launch. This has evolved somewhat and our current approach is described by Gautier et al. (2010). The key features are: 1) carry out high resolution reconnaissance spectroscopy to determine the stellar properties and the star’s suitability for radial-velocity work, and to search for signs of

---

<sup>1</sup>The time series photometry and radial velocity data, including bisector spans, may be retrieved from the MAST/HLSP data archive at [http://archive.stsci.edu/prepds/kepler\\_hlsp](http://archive.stsci.edu/prepds/kepler_hlsp).

stellar companions; 2) search for faint blended eclipsing binaries through the centroid shift approach (Batalha et al. 2010) and by means of high resolution imaging; and 3) detect the stellar reflex motion with precise radial-velocity measurements. In the future we hope to improve our constraints on stellar properties by including both asteroseismology results for at least the brighter host stars (Gilliland et al. 2010a) and parallaxes (Monet et al. 2010) for every target. These results are not available for Kepler-6 at this time.

### 3.1. Reconnaissance Spectroscopy

The reconnaissance spectra for Kepler-6 were carried out very early in the follow-up program, so observations were obtained with several of our resources for comparison purposes: the TRES spectrograph on the Tillinghast telescope (by L. Buchhave and D. Latham), the McDonald 2.7-m Coude spectrograph (by M. Endl and W. Cochran), and the FIES spectrograph on the Nordic Optical Telescope (by L. Buchhave and G. Fűrész). The spectra indicated that Kepler-6 was well suited for precise radial-velocity work and no evidence of double lines or a stellar companion was seen. The best data on stellar properties were determined later and are discussed below.

The mean radial velocity of Kepler-6 was determined by C. Chubak with two HIRES spectra using telluric lines to set their zero point. Observations of the radial velocity standard HD182488 using the same approach produced a mean value of  $-21.50 \pm 0.18 \text{ km s}^{-1}$ , in good agreement with the adopted value of  $-21.508 \text{ km s}^{-1}$ . Observations with FIES and TRES using the same standard star to determine their zero points were in good agreement with the HIRES velocity. The average of these values is shown in Table 2.

### 3.2. High-Resolution Imaging and Centroid Motion

Kepler-6 has a companion  $4.1''$  distant and 3.8 magnitudes fainter as seen in both a HIRES guide camera image and a PHARO  $J$  band AO image obtained with the Palomar Hale telescope (Gautier and Ciardi). A WIYN speckle image (Howell) shows only a single star within its  $2''$  square box. There are apparently two additional components both approximately 5.4 magnitudes fainter and  $11.5''$  distant that appear in the KIC as KIC IDs 10874615 and 10874616. These two objects refer to a single star and erroneously appear as two objects in the KIC. This star is very close to the edge of the aperture containing Kepler-6. The observed shift in the *Kepler* intensity weighted mean image centroid during transit,  $(-0.1, +0.3)$  millipixels in the (column, row) directions is consistent with the expected shift

if the faint companions are not the source of the transit signature. If the fainter, more distant star is fully in the aperture the expected shift is (0.0, +0.3) millipixels and if it is completely out of the aperture the expected shift is (−0.1, +0.4) millipixels, both being consistent with the observed centroid shift. On the other hand if the closer, brighter background star is the transit source the expected shift is 30 times larger, ruling out this possibility. The fainter object is too faint to produce the observed transit depth even if it disappears entirely during the transit, and if it could the resulting centroid shift would be nearly a factor of 100 larger than the observed shift. The typical sensitivity level for detection of centroid shifts is on the order of 0.1 millipixel or somewhat less. See Batalha et al. (2010) for a detailed discussion of this approach for candidate vetting.

### 3.3. PRECISE RADIAL VELOCITIES

Precise velocities were obtained by using HIRES on the Keck 1 telescope with iodine cell radial-velocity reference. A modified version of the standard HIRES iodine cell reduction pipeline that includes improved cosmic ray rejection and sky brightness suppression was applied to these spectra by J. Johnson. The reduction pipeline modification was necessary because of the faintness of this star compared to the bright stars normally observed for radial velocity planet search work. The nearby companion mentioned earlier is sufficiently far away on the sky that it does not interfere with the HIRES work. The phased velocities are shown in Figure 2 with a fit to a circular orbit whose phase and period are fixed by the observed transit times.

The Monte Carlo analysis described below shows no evidence of orbital eccentricity. In this analysis the eccentricity and longitude of periastron were parameterized as  $e \sin \omega$  and  $e \cos \omega$ . The probability distribution for these parameters is symmetrical with zero mean and a standard deviation of 0.029.

The rms of the velocity residuals is  $5.7 \text{ m s}^{-1}$  with the point nearest transit omitted from the fit. This point is potentially affected by the Rossiter-McLaughlin effect. Its residual of  $12 \text{ m s}^{-1}$  is larger than all the other velocity points and is in the sense of a prograde orbit. The rotational velocity given in Table 2 would result in an R-M amplitude of  $20 \text{ m s}^{-1}$ , certainly detectable with further careful spectroscopy. An analysis of the line bisectors (Figure 2) shows an rms of  $6.8 \text{ m s}^{-1}$  with no organized structure that might result from a triple system (Mandushev et al. 2005).

#### 4. DISCUSSION

A Monte Carlo bootstrap procedure developed by Rowe and Brown, outlined in Koch et al. (2010b) and Borucki et al. (2010b), that simultaneously fits the light curve and the radial velocities, and that is consistent with stellar evolution models, was carried out to produce most of the stellar and planetary properties presented in Table 2. The model light curve (Mandel & Agol 2002) was integrated over the long cadence integration period prior to fitting to the *Kepler* data. We note that the nearby companion star alluded to earlier is only about one *Kepler* pixel away from Kepler-6, so its light is included in the *Kepler* aperture. The fainter, more distant star is partially included in the aperture as well. This has the effect of diluting the depth of the transit by  $3.3 \pm 0.4\%$ . This effect has been taken into account in the modeling process including the dilution uncertainty due to the partial inclusion of the more distant star. The derived planetary density,  $0.352_{-0.022}^{+0.018}$  g cm<sup>-3</sup>, places it in a well-populated area of the mass-radius relationship for currently known extrasolar planets.

Several spectra obtained with HIRES without the iodine cell were subjected to an SME analysis (Valenti & Piskunov 1996) by D. Fischer to provide the remaining stellar properties reported in Table 2. In this analysis  $\log g$  was frozen at the transit-derived value since it is more reliable than the SME value, which was 4.59 if allowed to float. The discrepancy between the transit value of  $\log g$  and the SME value is significant. Gilliland et al. (2010b) and Nutzman et al. (2010) find a similar effect in their comparison of  $\log g$  derived from transit fits, asteroseismology constraints, and SME spectral analysis in the case of HD17156 ([Fe/H] = +0.24). In that case the discrepancy in  $\log g$  is smaller, 0.12, but is in the same sense. Bakos et al. (2009) find a similar situation for HAT-P-13 ([Fe/H] = +0.41) with a  $\log g$  discrepancy of +0.14. This suggests that there is a systematic error in the  $\log g$  values derived from SME analysis for high metallicity stars. However, Burke et al. (2007) find only a small  $\log g$  discrepancy of +0.02 in the case of XO-2 ([Fe/H] = +0.45) and the discrepancy for HD80606 ([Fe/H] = +0.4) is only +.01 (Naef et al. 2001; Winn et al. 2009). Further comparisons of spectroscopic  $\log g$  values with precise values derived from transits and asteroseismology are likely to be fruitful.

Funding for this Discovery mission is provided by NASA’s Science Mission Directorate.

It is with pleasure that we acknowledge the outstanding work done by the entire *Kepler* team during development, launch, commissioning, and the ongoing operations of the *Kepler* mission. It is an honor and a privilege to work with such a talented and dedicated group of people.

We thank the anonymous referee for several excellent suggestions that improved the paper.

*Facilities:* The Kepler Mission, Tillinghast (TRES), NOT (FIES), McDonald 2.7-m (Coude Spectrograph), Keck:I (HIRES), WIYN (Speckle), Palomar Hale (PHARO/NGS)

## REFERENCES

- Bakos, G. Á., et al. 2009, ApJ, in press (arXiv0907.3525B)
- Batalha, N., et al. 2010, ApJ, this issue
- Borucki, W. J., et al. 2010a, Science, Submitted
- Borucki, W. J., et al. 2010b, ApJ, this issue
- Burke, C. J., et al. 2007, ApJ, 671, 2115
- Gautier, T. N., et al. 2010, ApJ, this issue
- Gilliland, R. L., et al. 2010a, PASP, in press
- Gilliland, R. L., et al., 2010b, ApJ, Submitted
- Haas, M. R., et al. 2010, ApJ, this issue
- Jenkins, J. M., et al. 2010a, ApJ, this issue
- Jenkins, J. M., et al. 2010b, ApJ, this issue
- Koch, D. G., et al. 2010a, ApJ, this issue
- Koch, D. G., et al. 2010b, ApJ, this issue
- Latham, D. W. 2003. In Scientific Frontiers in Research on Extrasolar Planets, ASP Conf. Ser. 294, eds. D. Deming & S. Seager (San Francisco: ASP), 409
- Mandel, K., & Agol, E. 2002, ApJ, 580, L171
- Mandushev, G., et al. 2005, ApJ, 621, 1061
- Monet, D., et al. 2010, ApJ, this issue
- Naef, D., et al. 2001, A&A, 375, L27

Nutzman, P., et al. 2010, ApJ, Submitted

Valenti, J. A., & Piskunov, N. 1996, A&AS, 118, 595

Winn, J. N., et al. 2009, ApJ, 703, 2091



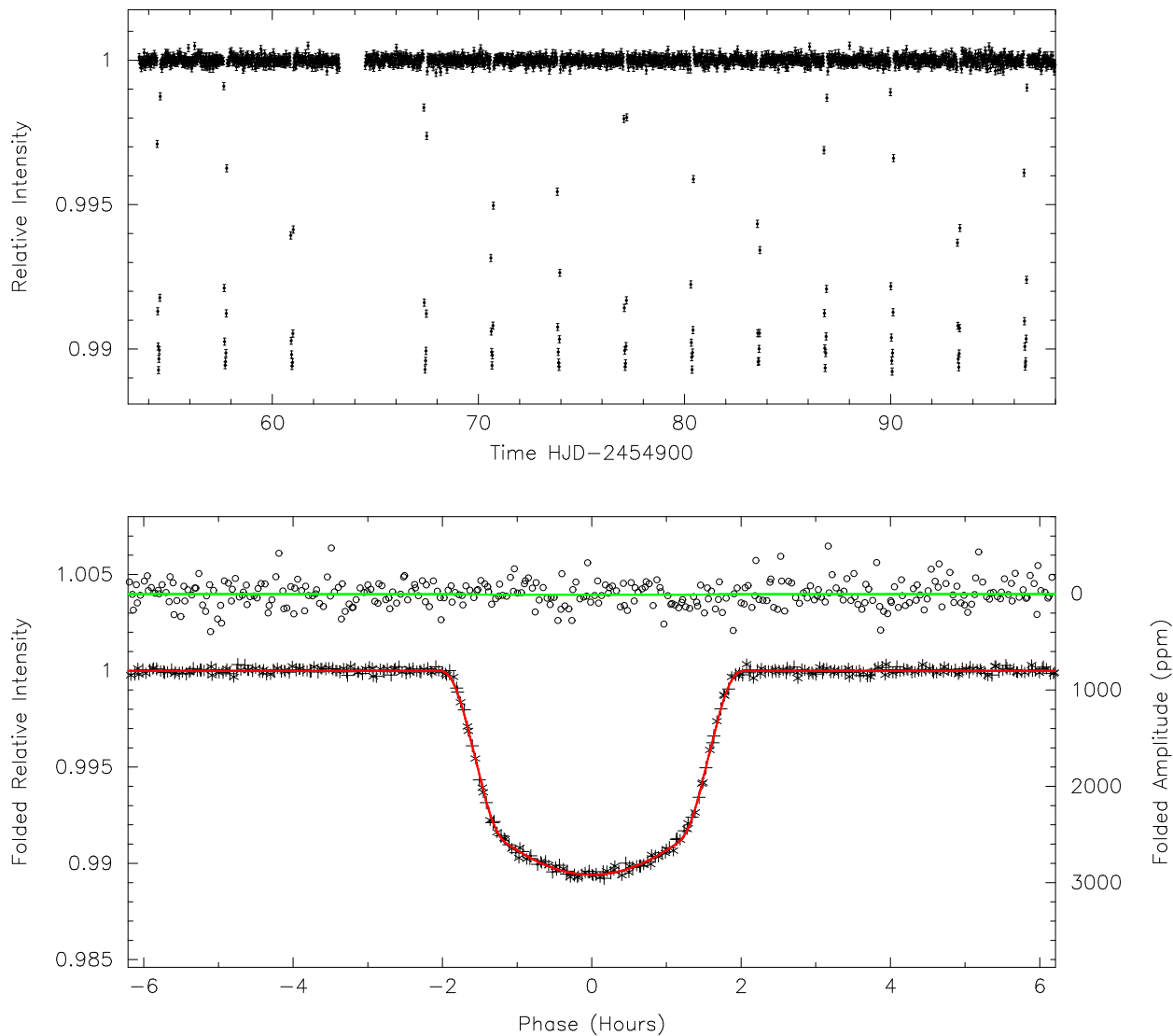


Fig. 1.— The detrended light curve for Kepler-6. The time series for the entire data set is plotted in the upper panel. The lower panel shows the photometry folded by the 3.234723-day period. The model fit to the primary transit is overplotted in red (vertical axis on the left), and our attempt to fit a corresponding secondary eclipse is shown in green with the expanded and offset scale on the right.

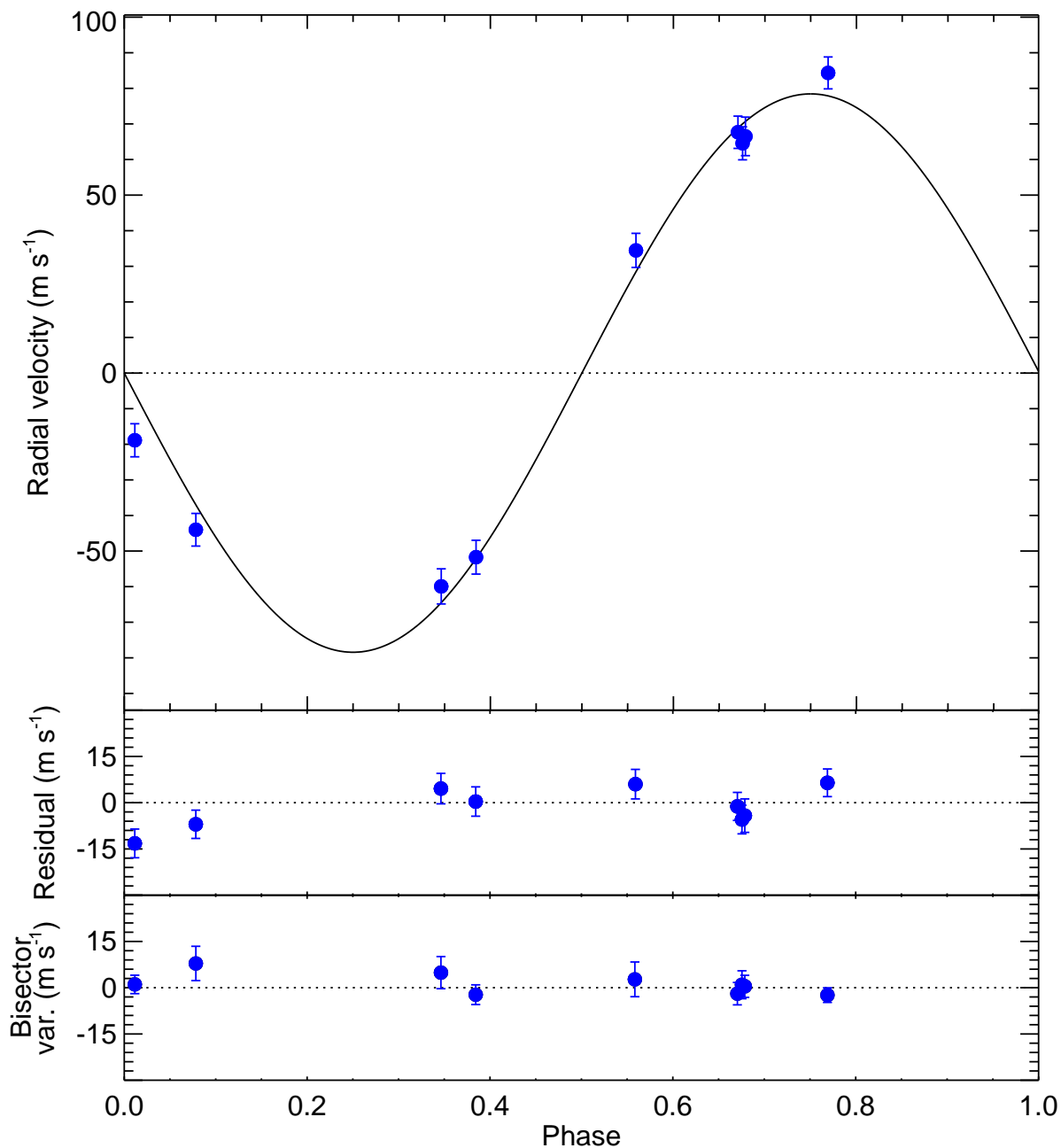


Fig. 2.— The orbital solution for Kepler-6. The observed radial velocities obtained with HIRES on the Keck 1 Telescope are plotted in the top panel together with the velocity curve for a circular orbit with the period and time of transit fixed by the photometric ephemeris. The middle panel shows the residuals to the fit. The point potentially affected by the Rossiter-McLaughlin effect is the one at the smallest phase. With this point omitted from the fit the rms of the residuals is  $5.7 \text{ m s}^{-1}$ . The lower panel shows the line bisector variation. No structure connected to the radial velocity curve is evident.

Table 1. Relative Radial-Velocity Measurements of Kepler-6

BJD	Phase	RV (m s <sup>-1</sup> )	$\sigma_{RV}$ (m s <sup>-1</sup> )
2454986.087289	0.769	+68.42	4.48
2454987.087348	0.078	-59.94	4.59
2454988.077695	0.384	-67.64	4.75
2454989.019649	0.676	+48.64	4.64
2454995.112273	0.559	+18.56	4.79
2455014.881155	0.671	+51.75	4.54
2455015.984052	0.012	-34.79	4.65
2455017.067098	0.346	-75.84	4.94
2455044.019956	0.679	+50.59	5.42

Table 2. System Parameters for Kepler-6

Parameter	Value	Notes
<i>Transit and orbital parameters</i>		
Orbital period $P$ (d)	$3.234723 \pm 0.000017$	A
Midtransit time $E$ (HJD)	$2454954.48636 \pm 0.00014$	A
Scaled semimajor axis $a/R_\star$	$7.05^{+0.11}_{-0.06}$	A
Scaled planet radius $R_P/R_\star$	$0.09829^{+0.00014}_{-0.00050}$	A
Impact parameter $b \equiv a \cos i/R_\star$	$0.398^{+0.020}_{-0.039}$	A
Orbital inclination $i$	$86^\circ 8 \pm 0.3$	A
Orbital semi-amplitude $K$ ( $\text{m s}^{-1}$ )	$80.9 \pm 2.6$	A,B
Orbital eccentricity $e$	0 (adopted)	A,B
Center-of-mass velocity $\gamma$ ( $\text{m s}^{-1}$ )	$-18.3 \pm 3.5$	A,B
<i>Observed stellar parameters</i>		
Effective temperature $T_{\text{eff}}$ (K)	$5647 \pm 44$	C
Spectroscopic gravity $\log g$ (cgs)	Fixed at transit value	C
Metallicity [Fe/H]	$+0.34 \pm 0.04$	C
Projected rotation $v \sin i$ ( $\text{km s}^{-1}$ )	$3.0 \pm 1.0$	C
Mean radial velocity ( $\text{km s}^{-1}$ )	$-49.14 \pm 0.10$	B
<i>Derived stellar parameters</i>		
Mass $M_\star (M_\odot)$	$1.209^{+0.044}_{-0.038}$	C,D
Radius $R_\star (R_\odot)$	$1.391^{+0.017}_{-0.034}$	C,D
Surface gravity $\log g_\star$ (cgs)	$4.236 \pm 0.011$	C,D
Luminosity $L_\star (L_\odot)$	$1.99^{+0.24}_{-0.21}$	C,D
Age (Gyr)	$3.8 \pm 1.0$	C,D
<i>Planetary parameters</i>		
Mass $M_P (M_J)$	$0.669^{+0.025}_{-0.030}$	A,B,C,D
Radius $R_P (R_J, \text{equatorial})$	$1.323^{+0.026}_{-0.029}$	A,B,C,D
Density $\rho_P$ ( $\text{g cm}^{-3}$ )	$0.352^{+0.018}_{-0.022}$	A,B,C,D
Surface gravity $\log g_P$ (cgs)	$2.974^{+0.016}_{-0.022}$	A,B,C
Orbital semimajor axis $a$ (AU)	$0.04567^{+0.00055}_{-0.00046}$	E
Equilibrium temperature $T_{\text{eq}}$ (K)	$1500 \pm 200$	F

Note. —

A: Based on the photometry.

B: Based on the radial velocities assuming an elliptical orbit.

C: Based on an SME analysis of the HIRES spectra.

D: Based on the Yale-Yonsei stellar evolution tracks.

E: Based on Newton's version of Kepler's Third Law and total mass.

F: Assumes Bond albedo = 0.1 and complete redistribution. The uncertainty reflects the uncertainties in these assumptions.